Cavitation Scaling Experiments With Headforms: Bubble Acoustics

Y. Chizelle[1], S. Ceccio[2], C. Brennan[1], Y. Shen[3]
([1]California Institute of Technology, USA; [2]University of Michigan, USA;
[3]David Taylor Model Basin, USA)

ABSTRACT

Recently Ceccio and Brennen [1][2][3] have examined the interaction between individual traveling cavitation bubbles and the structure of the boundary layer and flow field in which the bubble is growing and collapsing. They were able to show that individual bubbles are often fissioned by the fluid shear and that this process can significantly effect the acoustic signal produced by the collapse. Furthermore they were able to demonstrate a relationship between the number of cavitation events and the nuclei number distribution measured by holographic methods in the upstream flow. Kumar and Brennen [4][5] have further examined the statistical properties of the acoustical signals from individual cavitation bubbles on two different headforms in order to learn more about the bubble/flow interactions. All of these experiments were, however, conducted in the same facility with the same size of headform (5.08cm in diameter) and over a fairly narrow range of flow velocities (around 9m/s). Clearly this raises the issue of how the phenomena identified change with speed, scale and facility. The present paper will describe further results from experiments conducted in order to try to answer some of these important questions regarding the scaling of the cavitation phenomena. These experiments (see also Kuhn de Chizelle *et al.* [6][7]) were conducted in the Large Cavitation Channel of the David Taylor Research Center in Memphis Tennessee, on similar Schiebe headforms which are 5.08, 25.4 and 50.8cm in diameter for speeds ranging up to 15m/s and for a range of cavitation numbers.

NOMENCLATURE

C_p	pressure coefficient, $(P-P_o)/0.5\rho U_o^2$
D	headform diameter
I*	dimensionless acoustic impulse
P	static local pressure
P_o	static free-stream pressure
P_v	water vapor pressure
R	Radius of the base of the hemispherical cap of the bubble
Re	Reynolds number, U_oD/ν
t	time
Δt^*	dimensionless bubble travel time between electrodes 1 and 2
U_o	free-stream velocity
X_c	collapse coordinate along the axis of revolution
δ	bubble thickness in the direction normal to the headform surface
γ_i	dimensionless electrode duration parameter for electrode i
γ	global coverage parameter
ν	kinematic viscosity
ρ	density
σ	cavitation number, $(P_o-P_v)/0.5\rho U_o^2$
σ_i	inception cavitation number
τ_w	acoustic impulse duration

1. INTRODUCTION

The purpose of the experiments described herein is to investigate the effects of scale in the cavitation occurring on a simple axisymmetric headform. The focus is on traveling bubble cavitation, and the interaction between the flow and the dynamics and acoustics of individual bubbles. Experiments by Ceccio and Brennen [2][3] on 5.08cm diameter axisymmetric headforms had revealed a surprising complexity in the flow around single cavitation bubbles. Among the phenomena observed during those previous experiments were the fact that the bubbles have an approximately hemispherical shape and are separated from the solid surface by a thin film of liquid. This general conformation persists during the growth phase though, especially with the larger bubbles, the thin film appears to become unstable and may begin to shear off the underside of the bubble leaving a cloud of smaller bubbles behind. On the other hand, the collapse phase is quite complex and consists of at least three processes occurring simultaneously, namely collapse, shearing due to the velocity gradient near the

surface and the rolling up of the bubbles into vortices as a natural consequence of the first two processes. These processes tend to produce small transverse vortices with vapor/gas filled cores. It was noted that the collapse phase was dependent on the shape of the headform and the details differed between the ITTC headform (Lindgren and Johnson, [8]) which possesses a laminar separation and the Schiebe body (Schiebe, [9]; Meyer, Billet and Holl, [10]) which does not. The current investigation employed Schiebe headforms with a minimum pressure coefficient on the surface of Cp_{min}= -0.78.

Several other features of the flow around individual cavitation bubbles were noted in those earlier experiments and need to be mentioned here. On the ITTC headform, when some of the larger bubbles passed the point of laminar separation they would induce an attached "streak" of cavitation at both the lateral extremes of the bubble as indicated in Figure 1. These streaks would stretch out as the bubble proceeded downstream, being anchored at one end to a point on the body surface along the laminar separation line and at the other end to the "wing-tips" of the bubble. The main bubble would collapse, leaving the two streaks it induced to persist longer.

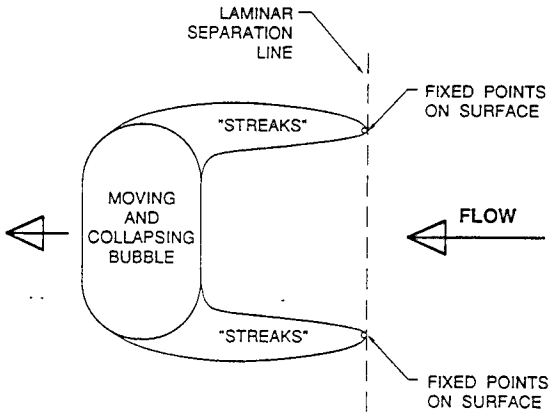

Fig. 1 Schematic diagram indicating the conformation of a cavitating bubble induced separation streaks.

One of the important consequences of these variations in the details of the collapse processes is the effect on the noise produced by a single cavitation event (Ceccio and Brennen, [2][3]; Kumar and Brennen, [4][5]). Bubble fission can produce several bubble collapses and therefore several acoustic pulses. Presumably this would also effect the cavitation damage potential of the flow. However it is important to reiterate that these earlier experiments were all conducted with 5.08cm diameter headforms and utilized only a very narrow range of tunnel velocities of 8-9m/s. Consequently there are very real questions as to how the observed phenomena might scale with both headform size and with tunnel velocity. The experiments described here represent one effort to answer some of these questions.

We digress briefly to note that questions on the scaling of cavitation have been asked for many years but particularly in the aftermath of the ITTC comparative tests conducted by Lindgren and Johnsson [8] who showed how disparate the appearance of cavitation was at different speeds, in different facilities and at different water "qualities". The latter characterization refers to the number of cavitation nuclei present in the water where most of these nuclei usually consist of very small air bubbles in the range of 5 to 300μm. As O'Hern *et al.* [11][12] have shown, the nuclei are similar in size distribution in most deaerated water tunnels and in the ocean. This causes one set of scaling questions since the ratio of body size to the nuclei size will change with the body size. The other set of scaling issues derives from the complex interactions between the bubbles and the flow close to the headform. Since the flow is Reynolds number dependent, scaling effects will also be caused by the changes in both body size and tunnel velocity. As a guide to interpretation of the results of the experiments a panel method was developed to solve the axisymmetric potential flow around the Schiebe headform in the absence of cavitation. Some results from these calculations are presented in Figure 2, which shows the isobars in the low pressure region on the surface of the headform.

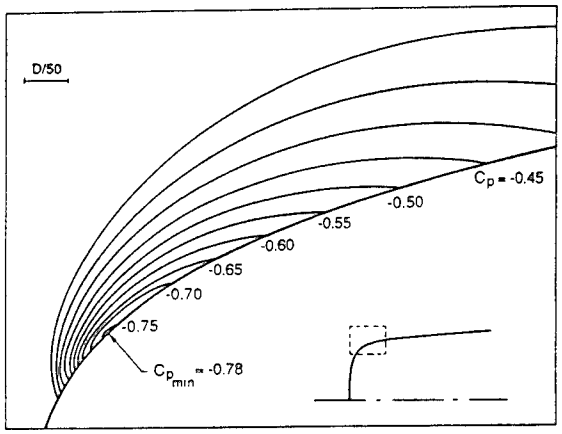

Fig. 2 Pressure distribution near the minimum pressure point in the potential flow around the Schiebe headform.

2. EXPERIMENTS

The data presented in this paper was taken during tests conducted in the Large Cavitation Channel of the David Taylor Research Center in Memphis, Tennessee (Morgan, [13]). Three geometrically similar axisymmetric Schiebe headform (Schiebe, [9]) measuring 5.08cm, 25.4cm and 50.8cm in diameter were installed on the centerline of the tunnel and cavitation tests were conducted over a range of tunnel speeds from 9m/s to 15m/s and dissolved oxygen contents (30 to 80% saturation at atmospheric pressure). The experimental

arrangements are described by Kuhn de Chizelle *et al.* in greater detail in other papers [6][7] and will not be repeated here. It is sufficient to indicate (i) that a larger number of still photographs and a substantial quantity of video was taken for each operating condition (the video was synched to a strobe light to improve time resolution), (ii) that surface electrodes were used to detect the presence of a bubble immediately over that electrode, (iii) that a hydrophone placed inside the headform recorded the cavitation noise (the headform was made of lucite and filled with water in order to provide a short and relatively reverberation free path for the noise between the cavitation and the hydrophone).

Figure 3 presents the observed cavitation inception numbers, σ_i, as a function of the headform diameter, D, tunnel velocity, U_o, and air content relative to saturation at atmospheric pressure. Inception was based on an arbitrarily chosen event rate of about 50 cavitation events per second. The events were detected by means of flush mounted electrodes, the current from which was moderated by the presence of a bubble [1][3].

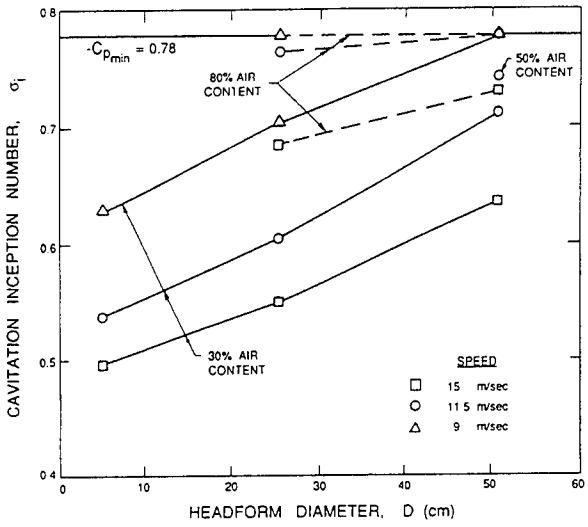

Fig. 3 Cavitation inception numbers σ_i, for the various headform sizes, velocities and air contents.

The trends in Figure 3 are fairly clear. The inception number increases with increasing headform size and the curves may well asymptote a value equal to the magnitude of the minimum pressure coefficient on the surface of the headform (Cp_{min}= -0.78). This headform size effect is simply a consequence of the fact that the larger the headform, the more nuclei are available for cavitation and, therefore, for a specific event rate the value of σ_i will be larger. The values of σ_i also increase with an increase in air content for a similar reason, namely more nuclei at the larger air contents. Figure 3 also demonstrates that the cavitation inception number increases with decreasing tunnel velocity. This effect is not so readily explained. However it is clear that to achieve the same cavitation number at a lower velocity one requires a lower tunnel pressure and it may be that the nuclei concentration in the tunnel increases considerably with decreasing operating pressure. We shall discuss this and other effects later in the paper.

3. EVENT RATE OBSERVATIONS

Both the photographs and the video tapes were analyzed in order to explore the variations in the cavitation event rates with headform size and tunnel velocity. The event rates were evaluated by counting the number of individual bubbles (or events) observable in a single frame and averaging this number over many frames. This allowed construction of Figure 4 in which the average number of observable events is plotted against the cavitation number, σ, for each of three velocities (9, 11.5 and 15m/s) for the three headforms (this data is for 30% dissolved oxygen content and we shall focus attention on these conditions). Not surprisingly the number of events increases with decreasing cavitation number and with increasing headform size. Not so predictable is the tendency for the number of events to decrease with increasing speed.

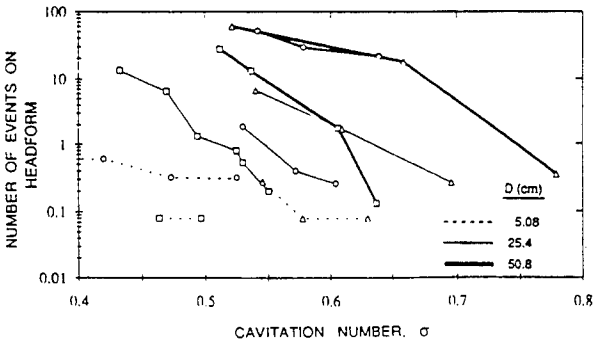

Fig. 4 Average number of observable events on the headform as a function of the cavitation number for all headform sizes and tunnel velocities.
□ U_o=15m/s; ○ U_o=11.5m/s; △ U_o=9m/s

The data on the number of events may be converted to cavitation event rates using bubble lifetimes obtained from knowledge of the velocity (from potential flow calculations using the panel method) and the measured locations of bubble appearance and collapse as a function of σ (see Kuhn de Chizelle *et al.*, [6]). The resulting event rate data for 30% dissolved oxygen content is presented in Figure 5 and it is clear that this is consistent with the cavitation inception data of Figure 3 given the selected criterion of 50 events/sec.

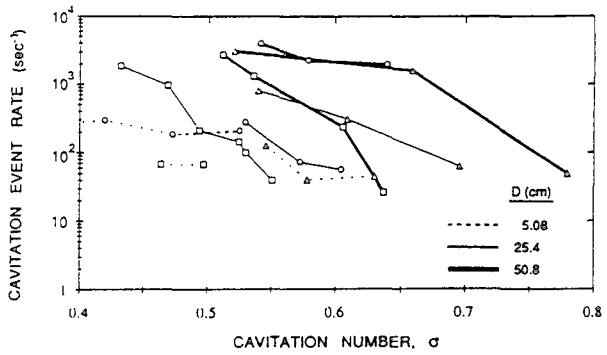

Fig. 5 Cavitation event rate as a function of the cavitation number for all headform sizes and tunnel velocities.

□ U_o=15m/s; ○ U_o=11.5m/s; △ U_o=9m/s

As previously stated, one of the purposes of the present investigations was to demonstrate the connection between the event rate (and by implication the inception number) and the nuclei number distribution. While the details of this analysis will be left until a later paper, it is instructive to present the event rate data of Figure 5 in the following modified form. Let us estimate that all the nuclei which pass through an annular stream-tube bounded on the inside by the headform and on the outside by the stream-surface which just touches the Cp=-σ isobar (see Figure 2) cavitate and therefore form observable bubbles. Then, using the potential flow velocity in this stream-tube (therefore neglecting boundary layer effects) and using the data of Figure 2 to estimate the thickness of the stream-tube at each cavitation number, we can calculate the volume flow rate of liquid in the stream-tube for each operating condition. Dividing the data of Figure 5 by these values we obtain an estimate of the number of cavitation nuclei per unit liquid volume; this data is presented in Figure 6.

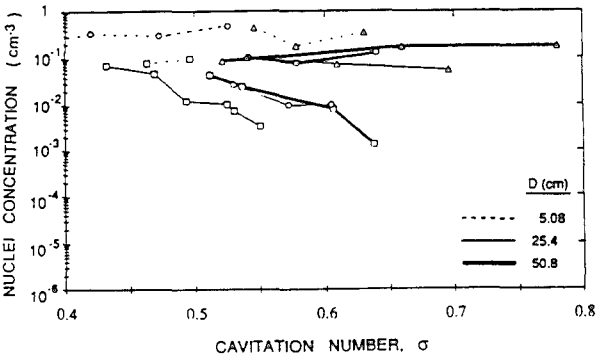

Fig. 6 Number of exited nuclei per unit liquid volume as a function of the cavitation number for all headform sizes and tunnel velocities.

□ U_o=15m/s; ○ U_o=11.5m/s; △ U_o=9m/s

It is significant that some of the variation with cavitation number, headform size and tunnel velocity which was present in Figures 4 and 5 has now been substantially removed. Indeed, with several exceptions, a fair fraction of the data of Figures 4 and 5 would now appear to correspond to a nuclei concentration of 0.1 nuclei/cm^3. The most noticeable deviation from this uniform value occurs at the highest speed (15m/s) with the two larger headforms.

The fact that most of the data appears to correspond to the same nuclei concentration is simultaneously encouraging and puzzling. It is encouraging because it suggests that a more careful analysis which begins with the same nuclei number distribution and follows each nucleus along its streamline may allow synthesis of the event rates and the inception numbers. But it is also puzzling because the concentration of 0.1 nuclei/cm^3 is at least an order of magnitude smaller than most of the measurements of cavitation nuclei would suggest.

Referring to Billet's [14] useful review of the subject of nuclei concentrations and distributions we note that the most reliable observations of nuclei (micro-bubbles and particles) have been obtained by systematically surveying the reconstructed holograms of volumes of tunnel water taken while the tunnel is in operation (for example Gates *et al.*, [15]). For de-aerated tunnel water, such inspections typically reveal concentrations of the order of 20 nuclei/cm^3 with sizes ranging from about 5μm to about 200μm. However the next question to ask is what fraction of these potential nuclei do, in fact, cavitate when subjected to sub-critical pressures. Here the answer is quite unclear. The other principal method for counting nuclei is the cavitation susceptibility meter in which the liquid is drawn through an orifice (or other device) in which the water is subjected to low pressures. The device is of sufficiently small size so that cavitation events occur individually. Then the concentration of actual cavitation nuclei (as opposed to potential nuclei) is obtained from the measured event rate and the known volume flow rate. Billet's review indicates that the typical concentrations measured by susceptibility meters is usually of the order of 2 nuclei/cm^3, significantly smaller than the concentrations obtained by holographic methods. While this may suggest that only a fraction of the potential nuclei actually cavitate, the data is, as yet, inadequate to support any firm conclusion.

In a later paper we shall present a model for the cavitation event rate which is based on a known nuclei number distribution function and follows all the possible sizes of nuclei along the streamlines on which cavitation might occur. This model is similar to that described by Ceccio [1] but corrects some errors in that previous analysis and includes other effects which may be important such as the effect of the boundary layer and the screening effect which occurs in the stagnation point flow and was first described by Johnson and Hsieh [16]. A brief preview of these results is given here. If one assumes a typical nuclei number distribution function, N(R) in m^{-4} of the form $N(R) = 10^{-5} / R^{3.5}$ for

$R < 2x10^{-4}$ m, then typical event rates for the Schiebe headform are shown in Figure 7. This data does not include the screening effect which reduces the event rate by about a factor 2 to 5. Nor does it include boundary layer effects which are small.

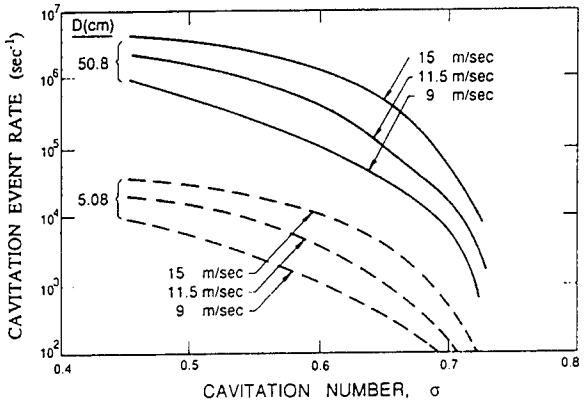

Fig. 7 Calculated event rates for the Schiebe headform for various headform sizes and tunnel velocities. Bubble screening effect not included.

Qualitative comparison of Figure 7 with Figure 5 reveals significant areas of both agreement and disagreement. Note first that the trend in event rate with headform size and with cavitation number are quite similar. However the trend with tunnel velocity produced by the model is contrary to the trend in most of the experiments. Perhaps this discrepancy is caused by assuming a common nuclei distribution for all operating conditions when, in fact, the nuclei population may be much higher at the low tunnel velocities than at the high since, to reach the same cavitation numbers, one must operate the tunnel at much lower pressures at the low velocities. The other area of disagreement to which reference was made earlier is that the event rates in the model are much higher than in the experiments.

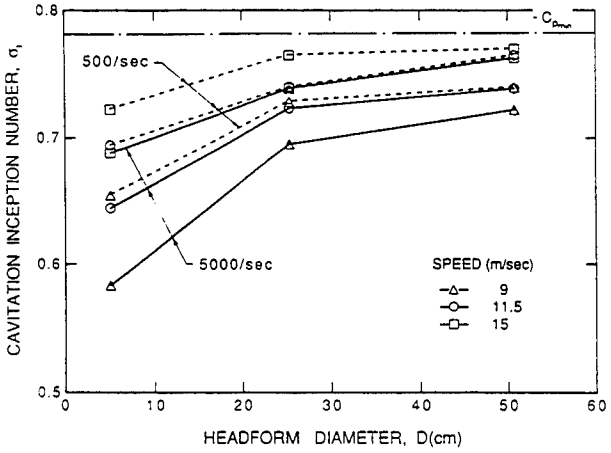

Fig. 8 Calculated cavitation inception numbers for various headform sizes and tunnel velocities and based on two different critical event rates of 5000/sec and 500/sec.

Given a model for the event rate one may the obtain cavitation inception numbers simply by establishing some critical event rate criterion. Figure 8 presents some typical cavitation inception numbers calculated in the way for criteria of 5000 events per second and 500 events per second. Comparing this with Figure 3 we note the same areas of disagreement that were manifest in the comparisons of event rates.

4. CAVITATION APPEARANCE

A typical bubble cavitation event consists of the growth and collapse of a bubble as it travels through the low pressure region close to the headform surface. The shape and size the bubble will assume are dependent on the cavitation number and the pressure coefficient history it experiences along its trajectory. In this section we shall describe in more detail the observations made during a study of the photographs and video recordings. The following observations were made at a dissolved oxygen content of 30%.

Bubble shape

For cavitation numbers close to the minimum pressure coefficient σ=0.78, the bubble life-time is very short. In Figure 3 we noted that the highest inception cavitation numbers occur for the largest bodies at the lowest velocities. Figure 9a shows a cavitation bubble for such conditions (σ_i=0.77; D=50.8cm; 9m/s; 30% dissolved oxygen content). All the bubbles assume a very thin disk-like geometry. For such cavitation numbers there is little or no growth normal to the headform surface. The bubbles grow almost entirely in the plane parallel to the headform. In its final phase the center of the bubble does not collapse first. Instead we observe the evanescence of the bubble's leading edge. There seems to be a location on the headform at which the cavity collapses, creating a fairly straight leading edge on the bubble. At these cavitation numbers we can see from Figure 2, that the critical isobar Cp=-σ is very elongated and close to the body surface. The region below vapor pressure is quite similar to the shape the bubbles assume. It appears that the bubbles are prevented from growing in the direction perpendicular to the body surface by the high normal pressure gradients normal to the surface. On the other hand, since the smallest headform has much smaller cavitation inception numbers (significantly less than 0.78), the bubbles observed on this headform do not assume such a flattened shape, even under inception conditions.

As the cavitation number is decreased below σ_i, the bubbles grow in volume (in diameter and in height) and assume the roughly hemispherical shape typified by Figure 9b. The maximum volume is mostly cavitation number dependent. As the bubbles approach their collapse phase their thickness, δ, normal to the headform surface decreases faster than their base radius, R, and the leading edge collapses most rapidly along a fairly straight

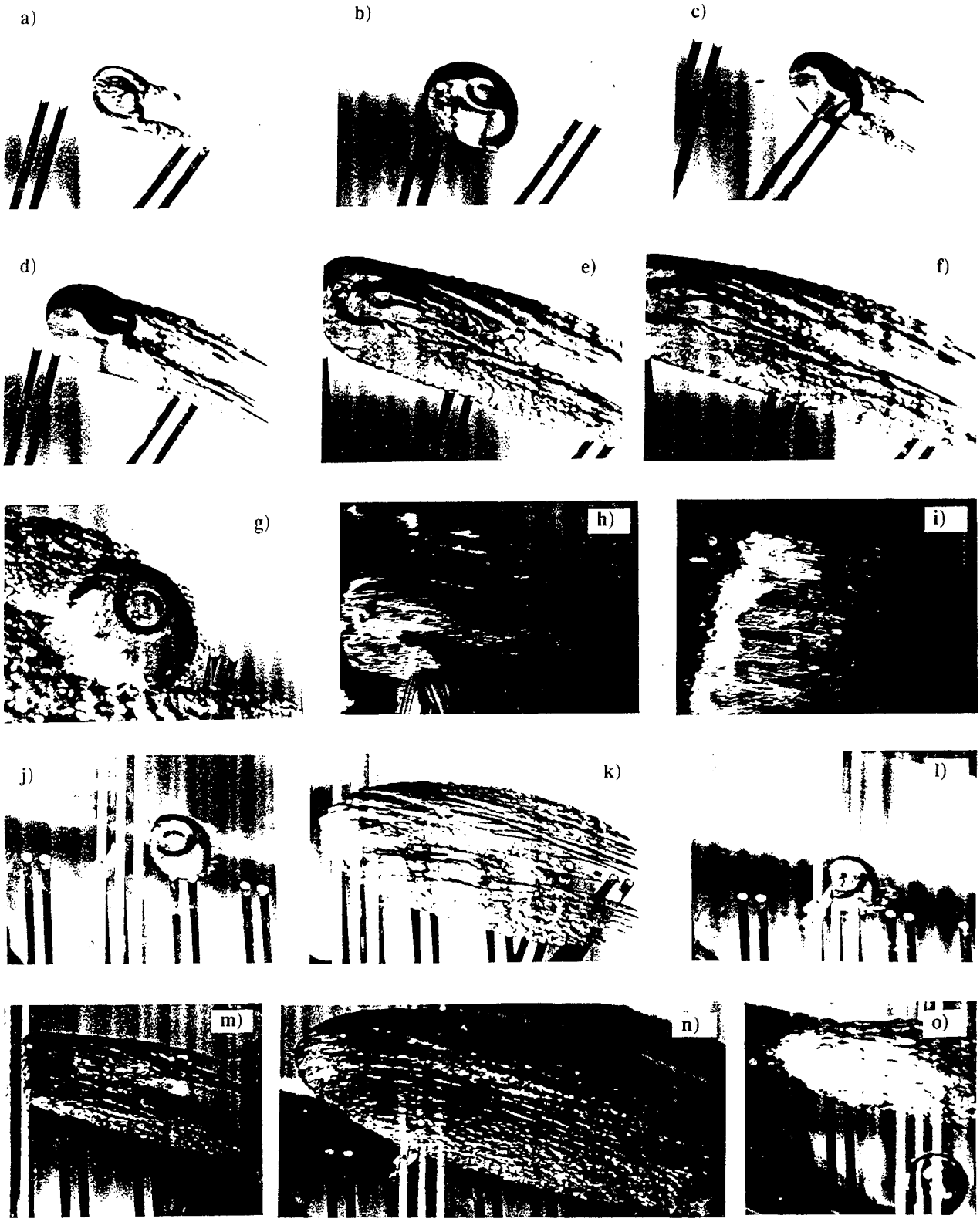

Fig. 9 High speed photography of cavitation events taken at a 30% saturation dissolved air content:
50.8cm diameter headform (distance between the two pairs of patch electrodes: 2.54cm) :
Figure **a**: U_O=9m/s, σ=0.77; Figures **b-c-d-e-f**: U_O=15m/s, σ=0.60; Figures **g-h**: U_O=15m/s, σ=0.54; Figure **i**: U_O=15m/s, σ=0.51
25.4cm diameter headform (distance between the two pairs of patch electrodes: 1.27cm) :
Figures **j-k**: U_O=15m/s, σ=0.55; Figures **l-m-n**: U_O=15m/s, σ=0.53; Figure **o**: U_O=15m/s, σ=0.49

front (Figures 9j, 9l). At this stage they appear thin and close to the headform surface (see also Ceccio, [1]) and look similar to the bubbles observed under inception conditions.

One unique feature of the present observations was the appearance of wave-like circular dimples on the top of the hemispherical cap (Figures 9b, 9e, 9f, 9g, 9j, 9l, 9m). The dimples seem to become more pronounced as the volume of the bubble increases. They are absent during the growth phase as seen in Figure 9c, and appear early in the collapse phase. Their ring shape could be interpreted as a precursor of a collapsing reentrant jet, but we note that the center of the dimple retains a concave curvature at all times. The dimple seems quite stable, and remains on the bubble until the very last stage of collapse. On the 50.8cm headform the dimples sometimes appear in pairs on the largest bubbles. On the smallest headform they do not form as distinctly, but occasionally a single rough depression in the center of the bubble may be observed.

Measurements of the bubbles on all three headforms show that the radius at the base of the hemispherical cap, R, scales linearly with the headform diameter, D (Kuhn de Chizelle *et al.*, [6]). At the same cavitation number, the ratio R/D, appears to be the same for all three headforms. We do not observe any variation of R/D with the velocity U_o. Furthermore the dimensionless collapse location X_c/D is approximately the same for all headforms. This appears to be true as long as the interactions between bubbles, or between bubbles and patch cavities remains limited. Therefore simple size scaling of the base diameter of the bubble cap with the headform size seems to be possible. This simple scaling applies only to the bubble's base radius though, since the shape of the bubble, its thickness δ, the amount of shear on its base and the cavitation event rate vary greatly from one headform to the other.

Bubble tail and patches

Figure 9a shows the presence of streaks of vapor or "tails" extending behind both sides of the bubble. It appears as though the bubble is sheared in the region extremely close to the headform surface leaving the tails behind in its wake. The undersides of some bubbles appear roughened towards the trailing and leading edges. The structure of the tails is always extremely wavy, turbulent and they seem to be attached to the headform surface (Fig. 9c). They appear early in the growth phase of the bubble. As the bubble is convected downstream it continues to "feed vapor" into the tails, allowing them to extend in length and height (Figures 9c, 9d, 9e, 9f). Ultimately the larger bubbles will collapse leaving behind patch-like cavities. It seems clear that whether a bubble will be sheared or not is determined early in the growth phase. If a bubble does not exhibit the trailing edge streaks early in its passage as seen in Figure 9c, it will grow and collapse with a smooth cap shape (Fig 9b, 9j, 9l). For this reason, for fixed cavitation conditions, the streaks always occur around the same position on the headform (Fig. 9c, 9d, 9e, 9f) and so will the leading edge of the patches. If the thickness of those streaks is small, the dynamic of the final collapse of the bubble appears unaffected by them and appears similar to the process described in the previous paragraph and seen in Figure 9m. However, for small enough cavitation numbers the patch can out-grow the bubble and swallow it leaving behind a patch-like cavity (Fig. 9k, 9n). At this point it is not clear if all the patch cavitation structures are generated by traveling bubbles. Some of them evidently are, and can be recognized by a planform shape, similar to a "V" with its vertex pointing downstream. The final length and thickness of the patch cavity are dependent on the bubble that generated it, and therefore vary with the headform diameter and cavitation number. For cavitation numbers close to the minimum pressure coefficient $-Cp_{min}=0.78$, no patches and very few bubble tails are observed as in Figure 9a. For these conditions the tails seem unable to grow sufficiently to form a patch-like cavity. Figures 9k, 9n show two typical patches at lower cavitation numbers. We notice that the patch on Figure 9k is thinner and ends sooner for higher cavitation numbers. The collapse mechanism of the patch itself is quite unclear. In the video recordings they vanish entirely between two frames (1/30 seconds). Is the entire patch swept downstream once the bubble head has vanished, or does it entirely collapse on the headform? The current investigation has not, as of yet, been able to answer these questions.

The number of sheared bubbles seems to increase with the cavitation number, headform diameter and flow velocity. Since the ratio of the laminar boundary layer thickness to headform size will scale with $Re^{-1/2}$, we would expect that the shearing of the cavitation bubbles would increase as the relative boundary layer thickness decreases. However, at the highest Reynolds number of 10^7, we note that the theoretical laminar to turbulent transition comes close to the low pressure region and might cause further disruptive effects.

Bubble-patch interactions

When the cavitation number is sufficiently reduced, the transient patches become fairly stable and remain on the headform, thus creating attached cavities for periods of up to a few seconds. As their number increases the patches will merge to create larger attached structures. Favre and Avellan [17] have shown that those attached cavities disturb the initial pressure distribution in such a way that they actually extend downstream beyond the original $Cp=-\sigma_i$ isobar. The cavitation number at which this phenomenon happens varies considerably from one headform to the other. It can be seen in Figure 9i at a cavitation number of about 0.5 for the 50.8cm headform. By contrast, at the same cavitation number, the 25.4cm headform produces just a few bubbles and patches (Figure 9o) and the 5.08cm headform shows no cavitation. At this point we note that the transient cavitation patch phenomenon was never observed on the smallest headform. That headform seems to exhibit an abrupt switch from traveling bubble cavitation (some of which have long trailing tails) to persistent attached

cavities. The attachment location of these cavities on that headform is fixed, and usually corresponds to a roughness element. This has not been observed on the larger headforms, even though the polished finish was identical to that of the 5.08cm body. Roughness appears to be a very critical parameter for the attached cavitation scaling of these bodies.

For all test conditions at cavitation number below 0.7 we noticed the coexistence of the two different kinds of cavitation patterns: traveling bubbles and transient patches. Quite remarkably, even for the conditions at which we observe many patch-type cavities, some very smooth hemispherical traveling bubbles are still present (Figure 9b, 9h). We can see in Figures 9g, 9h, 9i bubble type cavitation riding above attached cavities.

Comparing the shape of the bubbles encountering patch cavities with those which do not, it is clear that the shapes differ because the former are not subjected to the boundary layer shear which the latter experience. Bubbles which do encounter patches or attached cavities will eventually collapse and merge completely with the larger structure upstream of its closure region. By doing so they appear to perturb the attached cavity shape, as has been observed by Briancon-Marjollet *et al.* [18].

5. CAVITATION NOISE

For a range of cavitation numbers between inception and a value at which the cavitation patches persisted, it was possible to identify in the hydrophone output the signal produced by each individual bubble collapse. It was found necessary to digitally high pass filter the signals using a cut-off frequency of 5kHz in order to reduce the effect of vibration and noise caused by cavitation at the top of the supporting strut. This filtering did not, however, substantially effect the results. The processing amplifier gain response was calibrated and applied to the results. The noise from the cavitation was analyzed in several ways. We present first a spectral analysis which is the traditional approach normally taken toward cavitation noise. However more fundamental information can be gained from an analysis of the pressure pulses produced by individual cavitation events as will be described later.

Spectral analysis

FFT analyses of the signals from individual events were performed for different cavitation conditions for Nyquist frequencies up to 500kHz. In order to compare the shape of the power spectral density for different cavitating conditions the values have been non-dimensionalized by the number of sampled points, N, multiplied by the mean squared power amplitude, $\overline{PSD}$, where

$$\overline{PSD} = \frac{1}{N^2}\left[C^2(f_0) + C^2(f_{N/2}) + 2\sum_{i=1}^{i=N/2-1} C^2(f_i)\right].$$

The dimensionless PSD curves are presented in Figure 10 and consist of data averaged over several cavitation events.

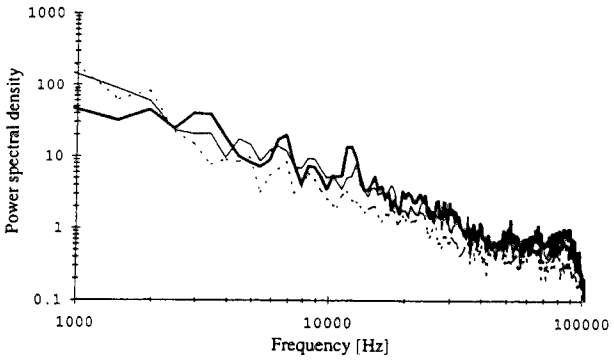

Fig. 10 Averaged dimensionless power spectral density signals for the 50.8cm headform:

——— U_o=9m/s, σ=0.66; ——— U_o=11.5m/s, σ=0.64; -------- U_o=15m/s, σ=0.61.

First we notice that for all headforms and tests conditions the measured spectral shape varies little with the operating condition and cavitation number as was reported by Arakeri and Shanmuganathan [19]. Most of the data represented here was taken close to inception. The influence of the hydrophone cutoff frequency above 80kHz can be observed in all signals. The measured decay between 1kHz and 80kHz in the present data appears roughly constant, with a value of about -22dB/dec. for all conditions. This value is similar to the value of -24dB/dec. (or $f^{-6/5}$) obtained earlier by Kumar and Brennen [5] and by Ceccio and Brennen [2][3] in the Caltech Low Turbulence Water Tunnel. By way of comparison we note that the spectra obtained by Blake *et al.* [20] for cavitation on a hydrofoil show a comparable frequency dependence of -20dB/dec. (or f^{-1}) though there is also a consistent dip in their spectra at 10kHz. Arakeri and Shanmuganathan [19] have presented data with a similar frequency dependence though the slope also increases from about -12dB/dec. (or $f^{-3/5}$) to -30dB/dec. (or $f^{-3/2}$) as the bubble interactions increase. None of this data is very close to the value of -8dB/dec. which Fitzpatrick and Strasberg [21] predicted for the range 10 to 100kHz based on a Rayleigh-Plesset analysis. Taking fluid compressibility into account yields decays as low as -40dB/dec. (f^{-2}) for the very high frequencies (around 100kHz and up), but these frequencies are beyond the capability of the hydrophone used in the present experiments.

Measurement of the frequency decay as a function of the cavitation number for different cavitating conditions is shown in Figure 11. We observe that this slope seems to decrease as the cavitation number value is reduced below 0.6. For some cavitation conditions the slope can be as low as -35dB/dec. This change is consistent with the effects of bubble interactions observed by Arakeri and Shanmuganathan [19].

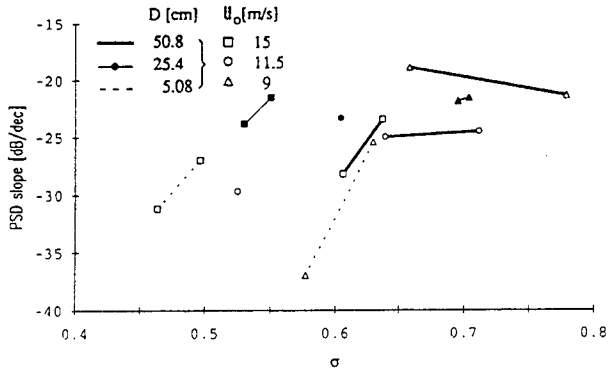

Fig 11. Average power spectral density slope decay between 1kHz and 80kHz [dB/dec.]. Measurements for different headform diameters and velocities as a function of the cavitation number.

Acoustic pressure pulses

The amplitudes of the acoustic pressure pulses were measured by defining the impulse, I, as the integral under that instantaneous pressure time history from the beginning of the collapse pulse to the moment when the pressure returns to its mean value. Since the impulse will vary inversely with the distance of the hydrophone from the noise source, we multiply I by the appropriate headform radius D/2 and form a dimensionless impulse, I*, by dividing by the headform radius, free stream velocity and the fluid density as indicated by the Rayleigh-Plesset analysis, so that the dimensionless impulse, $I^* = 4\pi I/\rho U_o$. The hydrophone output for each of the experimental conditions was examined in order to identify at least 40 of the larger pulses associated with a bubble collapse. The average values of the non-dimensional impulses obtained in this way are plotted against cavitation number in Figure 12.

The non-dimensional impulse is of the same order of magnitude for all three headforms. It initially increases as the cavitation number is decreased below inception. However most of the data also indicates that the average impulse ceases to increase and, in fact, decreases when σ is decreased below a certain value (about 0.43, 0.50 and 0.62 for the 5.08cm 25.4cm and 50.8cm diameter headform). The decrease at low cavitation numbers might be caused by the increasing presence of attached cavitation patches, damping the bubble collapse mechanism. The location of the peaks appears to be somewhat influenced by the velocity: they are shifted towards higher cavitation numbers for lower velocities. This trend is consistent with previous observations (Kuhn de Chizelle *et al.*, [6]) of the average void fraction over the headform at constant cavitation numbers, which exhibited an increase with a decrease in velocity. The conditions at which the impulses, I*, are maximum seem to correspond to circumstances in which the cavities cover about 20% of the surface area of the headform in the neighborhood of the minimum pressure point. Higher void fractions increase the interactions between the bubbles and the patches and considerably reduce the acoustic impulse. Such an effect was previously reported by Arakeri and Shanmuganathan [19] who noticed strong interaction effects for void fraction values larger than 25%.

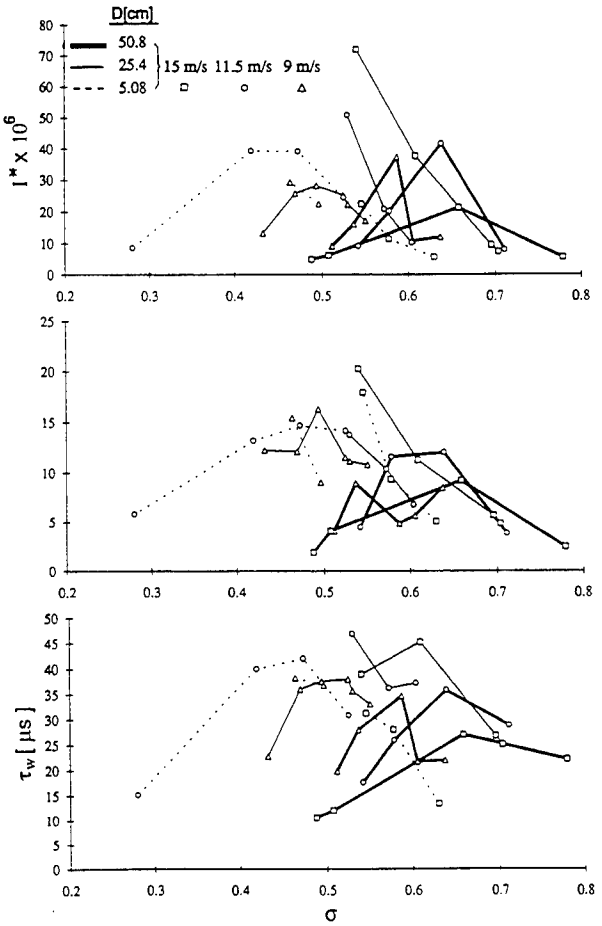

Fig. 12 Average dimensionless maximum acoustic impulse I*, standard deviation and impulse duration τ_w [μs] for all three headforms as a function of the cavitation number.

The standard deviation for the impulse is substantial, around 40% of the average value. Therefore for identical cavitation conditions the cavitation noise may vary considerably from one event to another. The duration of the impulse, τ_w, is also presented in Figure 12 and reveals a cavitation number dependence similar to that observed for the impulse. It appears to be of the same order of magnitude for all velocities and diameters. Examining this data it should be recalled that the typical response time of the hydrophone is about 3μs and is not negligible compared with the measured duration.

In summary, we find that the acoustic impulse produced by a single bubble collapse, while exhibiting considerable variability, nevertheless scales with headform size and tunnel velocity in the way which is expected on the basis of the Rayleigh-Plesset analysis.

Moreover, when the bubble concentration exceeds a certain value the noise from individual events becomes attenuated.

Electrode signal analyses

When a bubble is located over a particular electrode denoted by the index "i", it produces a perturbation in the voltage signal, $v_i(t)$, from that electrode. Figure 13 presents an example of the signals from the first and second patch electrodes (located at axial distances of 5.08 and 7.62cm from the headform stagnation point). The corresponding noise signal is plotted on the same Figure, time shifted by 170μs which corresponds to the time necessary for the acoustic noise to travel from the headform surface to the hydrophone. The signals from an unsheared bubble (seen in photograph 9b) and from a sheared bubble developing attached streaks (seen in photograph 9d) are contrasted in this Figure.

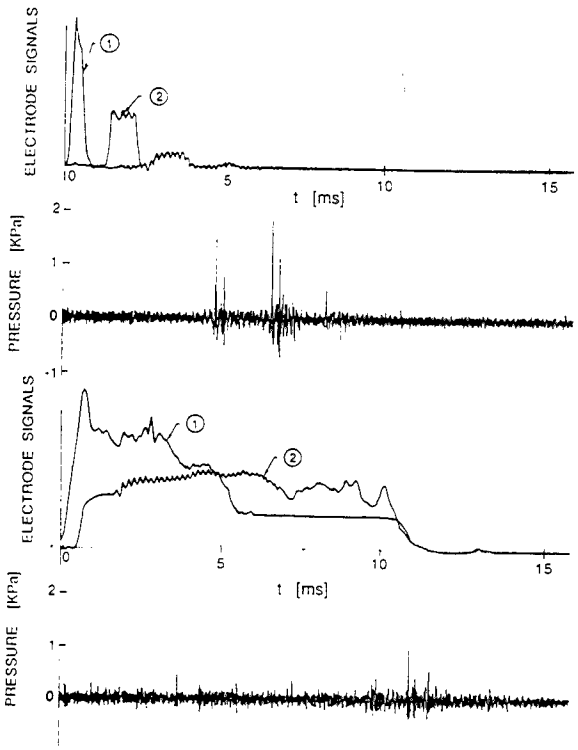

Fig. 13 Electrode signals from upstream patch electrodes 1 and 2 and the corresponding acoustic noise signals. The signals plotted correspond to the bubbles presented in photographs 9b and 9d.

Analyses of these electrode signals shed additional light on the mechanism of the bubble collapse. Sheared bubbles produce much longer electrode signals. Moreover, the trace from the first electrode will vanish before that from the second electrode, indicating that the collapse mechanism always proceeds in a downstream direction. Whether the cavity disappears by collapsing on the headform itself or detaches and is convected away by the flow is unclear. The time interval between the ends of the two electrode signals is often comparable to that measured for the case of unsheared traveling bubbles. This suggests that the leading edge of the patch detaches first and cavity is convected away by the flow.

The typical time for which a bubble covers an electrode is given by

$$\tau_i = \int_{t=0}^{t=\text{end of electrode signal}} v_i(t)dt \Big/ v_{i_{max}}$$

and can be written in dimensionless form by defining an electrode signal duration parameter $\gamma_i=\tau_i U_o/D$. Clearly a bubble with attached streaks or patches will yield substantially larger γ_i values than single unattached bubbles. Therefore γ_i provides a valuable indicator of the type of event which has occurred. The global coverage parameter γ defined as $\gamma = \sqrt{\gamma_1\gamma_2}$ groups both electrode duration parameters. Non-sheared bubbles typically have coverage parameters less than 0.01.

For single traveling bubbles, the duration parameters over the first and the second upstream patch electrode are strongly correlated. Figure 14 represents a plot of γ versus the dimensionless electrode duration for the first electrode, γ_1 ,for a wide range of cavitation numbers and velocities. Clearly there exists a strong correlation between both electrodes durations γ_1 and γ_2. It follows that a long (or short) duration at the first electrode leads to a long (or short) duration at the second electrode. Therefore we may conclude from Figure 14 that trailing streaks or tails (which cause larger durations) only appear early in the bubble evolution and that, if they do not appear, the bubble will continue without tail for the rest of its lifetime. This was also the conclusion reached from studies of photographs and video observations (Kuhn de Chizelle *et al.*, [6][7]). Note that the above implies that the leading edges of the attached patches are always upstream of the first electrode.

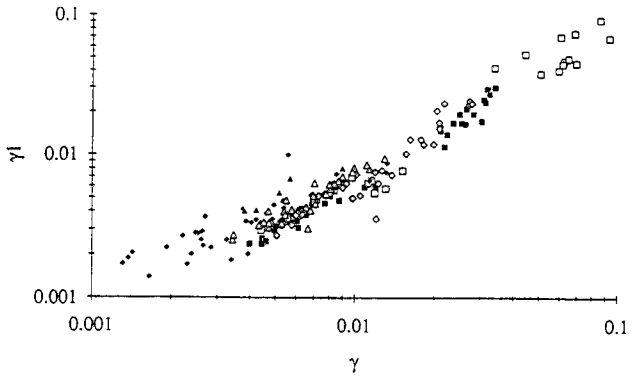

Fig. 14 Non-dimensional electrode signal duration time on the first and second patch electrodes for all flow velocities and cavitation numbers

The time of passage over the electrode "i" is denoted by t_i and may be defined by the quantity

$$t_i = \int_{t=0}^{t=\text{end of signal}} v_i(t)t\,dt \Big/ \int_{t=0}^{t=\text{end of signal}} v_i(t)\,dt.$$

Then the non-dimensional interval (or bubble travel time) between the signals from electrodes 1 and 2 can be defined as $\Delta t^*=(t_2-t_1)U_o/D$ and data on this quantity is presented in Figure 15.

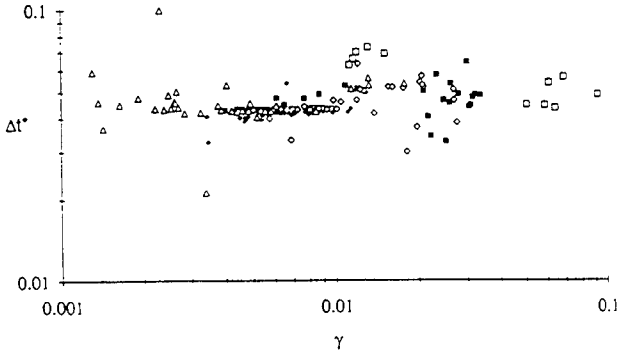

Fig. 15 Non-dimensional electrode peak interval, Δt^*, for all flow velocities and cavitation numbers.

For all conditions the non-dimensional interval is concentrated around a value of $\Delta t^*=0.043$. Panel method calculations of the non-dimensional travel time along a streamline between electrode 1 and electrode 2 yield an identical value of $\Delta t^*=0.043$ for the streamline closest to the headform. Also the travel time increases slightly as the streamline is located further from the headform. From the photographs Kuhn de Chizelle *et al.* [6] estimated that a typical non-dimensional bubble thickness for cavitation numbers around 0.65 is about $\delta\approx 0.01$ and the potential flow travel time for streamlines located at that distance above the headform surface is $\Delta t^*=0.044$. The agreement between the measured travel time for non-sheared bubbles (represented by γ values less than 0.01) and the potential flow calculation indicates that there is no slip between the bubble and the inviscid flow outside the boundary layer. The bubbles appear to ride over the boundary layer and travel at the same velocity as the outer flow.

For shear factors less than 0.005 which correspond to the highest cavitation numbers ($\sigma \geq 0.70$) some scatter can be observed. For those conditions photographs indicate that many bubbles collapse before they reach the second electrode. The signals measured on the second electrode may therefore be generated by rebounded bubbles. At the other extreme the large values of γ (>0.01) correspond to long sheared bubbles with tails. Note from Figure 15 that the scatter in Δt^* increases significantly with γ and that there is a trend toward greater travel times indicating that the bubble velocity is slower than that of the flow outside the boundary layer. This is consistent with part of the bubble being within the boundary layer.

Since the electrodes and the hydrophone signals were recorded simultaneously, it is possible to correlate the acoustic output of each event with the γ value for that event in order to explore the effect of bubble attachment on the noise. Figure 16 presents γ as a function of the non-dimensional acoustic impulse, I*, for the 50.8cm headform at 30% dissolved oxygen content. Most of the data is confined to cavitation numbers close to inception (low event rates) in order to ensure no overlap between events.

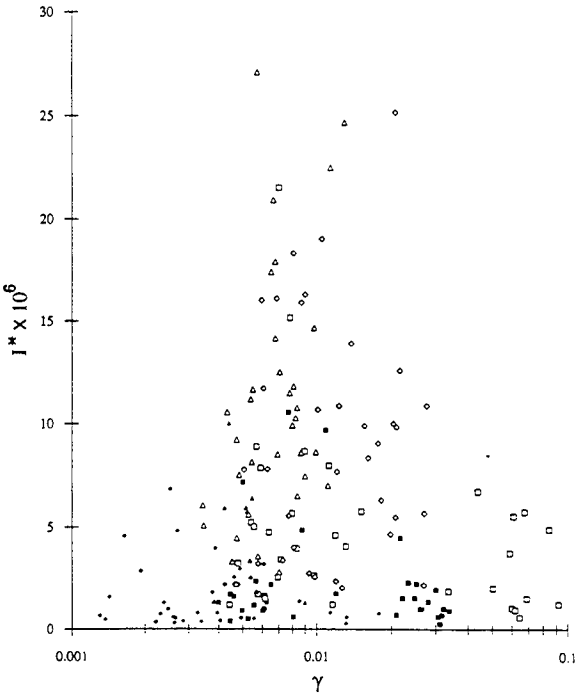

Fig. 16 Dimensionless acoustic impulse, I*, for the 50.8cm headform as a function of the electrode signal coverage parameter γ.

- ■ σ=0.64, U_o=15m/s; □ σ=0.60, U_o=15m/s;
- ◆ σ=0.71, U_o=11.5m/s ◇ σ=0.64, U_o=11.5m/s;
- ▲ σ=0.78, U_o=9m/s; △ σ=0.66, U_o=9m/s

Figure 16 leads to several conclusions. First we focus on the data on the left hand side for values of γ less than 0.01. These correspond to unattached bubbles with the smallest bubbles having the smallest values of γ. In this regime the impulse increases with increasing γ (i.e. decreasing cavitation numbers and increasing bubble size) as previously suggested by many authors, for example Fitzpatrick and Strasberg [21] and Hamilton *et al.* [22]. Ceccio and Brennen [2][3] also demonstrated that the impulse may be much smaller than this maximum. The data here clearly exhibit an upper bound

or envelope on the impulse. Vogel *et al.* [23] have also reported that the cavitation noise increases for the case of unsheared bubbles as the ratio of the distance to the headform and the maximum bubble radius decreases.

The present data adds to these earlier studies in that it shows a clear decline in the impulse when the value of γ exceeds about 0.02. These γ values correspond to bubbles which have attached streaks and patches and it is apparent that this results in a decrease in the impulse associated with the collapse of these events. The largest coverage parameters, γ, correspond to the lowest cavitation numbers and thus to the largest patch cavities. The reduction in cavitation noise for these types of events can probably be attributed to the fact that the collapse is much less coherent, producing high pressure nodes which are much smaller in magnitude.

6. CONCLUSIONS

In this paper we have presented some of the results from a series of experiments carried out in the Large Cavitation Channel (LCC) to investigate the scaling of the dynamics and acoustics of individual cavitation bubbles in flows around headforms. Many of the phenomena observed by Ceccio and Brennen [2][3] in experiments on 5.08cm headforms were seen again in the present experiments. Such micro-fluid mechanical phenomena included the hemispherical shape of individual cavitation bubbles, the thin film separating them from the surface, the destabilization of that film, the occasional production of attached streaks in the wake of the bubbles and the complex processes during the bubble collapse including bubble fission and roll-up into vortices.

The present experiments yielded substantially lower cavitation inception numbers for the larger headforms. One result of this was that for the same air content, velocity and cavitation number, we observed bubble inception on the smallest headform and fully developed attached cavitation on the largest. Some of the differences in the appearance of individual bubbles on the three headforms could be attributed to this large difference in inception numbers since it implied quite different locations for the critical C_p=-σ isobars. The most noticeable effect of scale on the appearance of cavitation was the increase in bubble-generated attached streaks and patches for the larger headforms. On the 5.08cm headform a traveling bubble would occasionally generate two attached streaks or tails at the lateral extremes of the bubble. These would disappear almost immediately after the bubble collapsed. On the larger headforms at higher speeds (larger Reynolds numbers) and low cavitation numbers the streaks began to occur more frequently and extend behind the entire width of the bubble. The streaks would tend to produce a transient patch of attached cavitation which would disappear shortly after the bubble collapsed. For low enough cavitation numbers , however, the patches would persist almost indefinitely and create larger attached cavitation structures. It is possible that this is the mechanism of formation for most patch cavitation.

Another new observation during the present experiments was the appearance of a remarkably repeatable "dimple" on the exterior surface of the traveling bubbles on the two larger headforms. These seem to appear when the bubble (or headform) is sufficiently large which suggests that the dimples are influenced by surface tension effects.

Cavitation event rates were also evaluated from the photographs and videotapes and this data clearly complements the observations of cavitation inception since inception was based on a chosen event rate. The event rates increase with increasing headform size and with decreasing cavitation number in the expected fashion if one assumes a fixed nuclei concentration. However the observed increase in the event rates with decrease in tunnel velocity are contrary to that which one would expect from the lower nuclei flux at lower speeds. It suggests that the nuclei population is substantially larger when the facility is operated at the lower pressures needed to achieve the same cavitation numbers at a lower velocity. It is also demonstrated that the event rates appear to correspond to a nuclei population of the order of 0.1 nuclei/cm^3 which is at least an order of magnitude lower than the expected nuclei population. We are continuing to investigate possible explanations for this discrepancy including the bubble screening effect first suggested by Johnson and Hsieh [16].

The noise generated by individual events and the variations in the noise with the type of event were also investigated. We first demonstrate that the acoustic impulse generated by individual traveling bubbles scales quite well with headform size and tunnel velocity and that this scaling is in accord with that expected from the Rayleigh-Plesset or Fitzpatrick-Strasberg analysis. As expected lower cavitation numbers lead to larger bubbles and larger impulses as long as the bubbles do not interfere with one another or with larger patch cavities.

As in the previous study by Ceccio and Brennen [2][3] the impulses generated are less than about a third of the magnitude predicted by the Rayleigh-Plesset analysis. It seems likely that the shearing and fission the bubble experiences prior to collapse leads to a less highly focused and less "efficient" noise-producing event. The present study has added to this information. We have shown that the events which generate attached "streaks" or "tails" and which represent a greater fraction of the events at higher Reynolds numbers also produce significantly smaller acoustic impulses. This correlation was observed by special cross-correlation of the surface electrode signals and the hydrophone output. The above observation has clear implications for the scaling of cavitation noise.

Some additional observations were made for those conditions at which the cavitation number was small enough for persistent attached patches to form and at which the void fraction of bubbles in the cavitation region became significant. First it was clear that when a traveling bubble encountered (or rode over) a patch its dynamics were altered and its acoustic output

substantially diminished. Secondly like Arakeri and Shanmuganathan [19] we also observed a significant decrease in the noise when the void fraction was sufficiently large so that the bubbles covered about 20% of the area in the cavitation region.

ACKNOWLEDGMENTS

Large scale experiments like these require help of many people and the authors are very grateful to all of those who helped in this enterprise. We are very grateful to the ONR for their support under contracts N00014-91-J-1426 (SLC) and N00014-91-J-1295 (CEB, YKdC). We are also extremely grateful to the David Taylor Research Center (DTRC) and to their staff including W.B. Morgan for making the use of the LCC possible for us and to both Scott Gowing and James Blanton of DTRC for extensive help with the experiments. Po-Wen Yu from the U. of Michigan also provided important help with the photography.

REFERENCES

1. Ceccio, S.L. 1989. "Observations of the dynamics and acoustics of traveling bubble cavitation." Ph.D. Thesis, California Institute of Technology.
2. Brennen, C.E. and Ceccio, S.L. 1989. "Recent Observations on cavitation and cavitation noise." Proc. ASME Third Int. Symp. on Cavitation Noise and Erosion in Fluid Systems, San Francisco, FED-Vol. 88, pp. 67-78.
3. Ceccio, S.L. and Brennen, C.E. 1991. "The dynamics and acoustics of traveling bubble cavitation." J. Fluid Mech., Vol. 233, pp. 633-660.
4. Kumar, S. and Brennen, C.E. 1991. "Statistics of noise generated by traveling bubble cavitation." ASME Cavitation and Multiphase Flow Forum, Portland OR, June 1991, FED Vol. 109, pp. 55-62.
5. Kumar, S. and Brennen, C.E. 1992. "An acoustical study of traveling bubble cavitation." Submitted to J. of Fluid Mech.
6. Kuhn de Chizelle, Y., Ceccio, S.L., Brennen, C.E. and Shen, Y. 1992. "Cavitation scaling experiments with headforms: Bubble dynamics." Proc. Second International Symposium on Propeller and Cavitation, Hangzhou, China.
7. Kuhn de Chizelle, Y., Ceccio, S.L., Brennen, C.E. and Shen, Y. 1992. "Scaling experiments on the dynamics and acoustics of traveling bubble cavitation." Proc. Institution of Mechanical Engineers, Cambridge, UK.
8. Lindgren, H. and Johnsson, C.A. 1966. "Cavitation inception on headforms. ITTC comparative experiments." Proc. 11th Int. Towing Tank Conf., pp. 219-232.
9. Schiebe, F.R. 1972. "Measurements of the cavitation susceptibility of water using standard bodies." St. Anthony Falls Hydraulic Lab., Univ. of Minnesota, Rep. No. 118.
10. Meyer, R.S., Billet, M.L. and Holl, J.W. 1989. "Free-stream nuclei and cavitation." Proc. ASME Third Int. Symp. on Cavitation Noise and Erosion in Fluid Systems, San Francisco, FED-Vol. 88, pp. 52-62.
11. O'Hern, T., D'Agostino, L. and Acosta, A.J. 1988. "Comparison of holographic and counter measurements of cavitation nuclei in the ocean." ASME J. Fluids Eng., Vol, 110, pp. 200-207.
12. O'Hern, T., Katz, J. and Acosta, A.J. 1985. "Holographic measurements of cavitation nuclei in the sea." ASME Cavitation and Multiphase Flow Forum Booklet, FED Vol. 23, pp 39-42.
13. Morgan, W.B. 1990. "David Taylor Research Center's Large Cavitation Channel." Proc. Int. Towing Tank Conference, Madrid, Spain, pp. 1-9.
14. Billet, M.L. 1985. "Cavitation nuclei measurement - A review." ASME Cavitation and Multiphase flow Forum, Booklet, pp. 31-38.
15. Gates, E.M., Billet, M.L., Katz, J., Ooi, K.K., Holl, W. and Acosta A.J. 1979. "Cavitation inception and nuclei distribution. Joint ARL-CIT experiments." Rep. E244-1, Calif. Inst. of Tech., Div. of Eng. and Appl. Sciences, Pasadena, CA 91125.
16. Johnson, V.E. and Hsieh, T. 1966. "The influence of gas nuclei on cavitation inception." Proc. Sixth Symposium on Naval Hydrodynamics, Washington D. C.
17. Favre, J.N., Avellan, F., Ryhming, I.L. 1987. "Cavitation performance improvement using a 2-D inverse method of hydraulic runner design." Proc. Int. Conf. on Inverse Design Concepts and Optimization in Engineering Science-II., Penn. State Univ.
18. Briancon-Marjollet, L. and Franc, J.M. 1990. "Transient bubbles interacting with an attached cavity and the boundary layer." J. Fluid Mech., Vol. 218, pp. 355-376.
19. Arakeri, V.H. and Shanmuganathan, V. 1985. "On the evidence for the effect of bubble interference on cavitation noise." J. Fluid Mech., Vol. 159, pp. 131-150.
20. Blake, W.K., Wolpert, M.J. and Geib, F.E. 1977. "Cavitation noise and inception as influenced by boundary layer development on a hydrofoil." J. Fluid Mech., Vol. 80, pp. 617-640.
21. Fitzpatrick, H.M. and Strasberg, M. 1956. "Hydrodynamic sources of sound." First Symp. on Naval Hydrodynamics, Washington D.C., pp. 241-280.
22. Hamilton, M.F., Thompson, D.E. and Billet, M.L. 1982. "An experimental study of traveling bubble cavitation and noise." ASME Int. Symp. on Cavitation Noise, pp. 25-33.
23. Vogel, A., Lauterborn, W. and Timm, R. 1989. "Optical and acoustic investigations of dynamics of the Laser-produced cavitation bubbles near a solid boundary layer." J. Fluid Mech., Vol. 206, pp. 299-338.